Effect of phase mismatch on second-harmonic generation in negative-index materials

Zh. Kudyshev, I. Gabitov, and A. Maimistov

Phys. Rev. A **87**, 063840 — Published 24 June 2013

DOI: 10.1103/PhysRevA.87.063840

The effect of phase mismatch on second harmonic generation in negative index materials

Zh. Kudyshev[1], I. Gabitov[2,3] and A. Maimistov[4]

[1] *Department of Physics, Al-Farabi Kazakh National University, al-Farabi ave., 71, Almaty, 050038, KAZAKHSTAN*

[2] *Department of Mathematics, the University of Arizona, 617 N. Santa Rita, Tucson, AZ 85721-0089, USA*

[3] *Department of Mathematics, SMU, 3200 Dyer Street, Dallas TX 75275-0156 , USA*

[4] *Department of Solid State Physics and Nanosystems, National research nuclear university MEPhI, Kashirskoe sh. 31, Moscow, 115409, RUSSIA*

Abstract

Second harmonic generation in negative index metamaterials is considered. Theoretical analysis of the corresponding model demonstrates a significant difference of this phenomenon in conventional and negative index materials. For example and in contrast to conventional materials, there is nonzero critical phase mismatch. The behavior of interacting waves is dramatically different when phase mismatch is smaller or greater than a critical value.

I. INTRODUCTION

Experimental demonstration of the phenomenon of negative index of refraction first in the microwave [1] and latter in the optical regime [2, 3] has stimulated growing interest in nonlinear properties of negative index materials [4]. This interest is motivated by specifics on the interaction of electromagnetic waves with negative index materials. In combination with a nonlinear response of the optical material to electromagnetic radiation, this interaction leads to new nonlinear optical phenomena. The study of these phenomena is of considerable importance both for better understanding of fundamentals of electrodynamics of negative index materials and for their applications. One of the most fundamental property of negative index material is an opposite directionality of the Poynting vector, characterizing the energy flux, to the wave vector $\vec{k}$. On the other hand, the negative index property can be realized only on particular wavelength intervals. These two features are offering a very unusual type of multi-wave interactions if frequencies of interacting waves correspond to frequency intervals where the optical material has different signs of refractive index. Multi-wave interaction must satisfy a phase matching condition, which is possible only when all wave vectors are pointed in the same direction [5]. Therefore energy fluxes of the waves with frequencies corresponding to a negative sign of refractive index will propagate in opposite direction to those with frequencies corresponding to a positive sign of the index of refraction.

Such effect was suggested for the first time in [7], which considered the particular case of three-wave interaction - second harmonic generation (see also [8–10]

A solution of the equations describing second harmonic generation in the case of exact phase matching was given in [21]. The feasibility of parametric amplification using three-wave interaction for compensation losses in negative index materials was studied in [20]. The dynamics of interacting wave packets propagating in negative index materials in the case of second harmonic generation was considered in [22, 23]. It was shown that in contrast to a weak intensity of the pump field, at high intensities a second harmonic pulse can be trapped by the pump pulse and forced to propagate in the same direction.

In this paper we investigate second harmonic generation in the presence of phase-mismatch Δ. This is an important case since phase-mismatch is more relevant to realistic experimental conditions. Additionally, it introduces two types of spatial distribution of the second harmonic field intensity along the sample: monotonic and periodic on the propagation

spatial coordinate. Both cases are considered in this paper. We also studied second harmonic generation near a critical phase-mismatch value, when the material becomes transparent for the pump wave.

II. BASIC EQUATIONS

The system of equations describing three wave interactions (one dimensional case) in a χ^2 - medium for the slowly varying envelope and phase approximation can be written in the following form [5, 11]:

$$\begin{aligned}
\left(\widehat{k}_1\frac{\partial}{\partial z}+\frac{1}{\vartheta_1}\frac{\partial}{\partial t}\right)A_1 &= \imath\frac{2\pi\omega_1^2\mu(\omega_1)}{c^2k_1}P^{NL}(\omega_1)\exp\left(-\imath k_1 z\right)\\
\left(\widehat{k}_2\frac{\partial}{\partial z}+\frac{1}{\vartheta_2}\frac{\partial}{\partial t}\right)A_2 &= \imath\frac{2\pi\omega_2^2\mu(\omega_2)}{c^2k_2}P^{NL}(\omega_2)\exp\left(-\imath k_2 z\right)\\
\left(\widehat{k}_3\frac{\partial}{\partial z}+\frac{1}{\vartheta_3}\frac{\partial}{\partial t}\right)A_3 &= \imath\frac{2\pi\omega_3^2\mu(\omega_3)}{c^2k_3}P^{NL}(\omega_3)\exp\left(-\imath k_3 z\right)
\end{aligned} \tag{1}$$

where wave numbers $k_j,\ j=1,2$ are defined as follows $k_j^2=\left(\omega_j/c\right)^2\varepsilon(\omega_j)\mu(\omega_j)$, $\widehat{k}_j$ is the sign of the square root of $n_j^2=\varepsilon(\omega_j)\mu(\omega_j)$ and

$$\begin{aligned}
P^{NL}(\omega_1) &= \chi^2(\omega_1;\omega_3,-\omega_2)A_3A_2^*\exp\left(\imath z(k_3-k_2)\right)\\
P^{NL}(\omega_2) &= \chi^2(\omega_2;\omega_3,-\omega_1)A_3A_1^*\exp\left(\imath z(k_3-k_1)\right)\\
P^{NL}(\omega_3) &= \chi^2(\omega_3;\omega_1,\omega_2)A_1A_2\exp\left(\imath z(k_1+k_2)\right)
\end{aligned} \tag{2}$$

For the case of second harmonic generation Eqs. (1) take the following form:

$$\begin{aligned}
\left(\widehat{k}_\omega\frac{\partial}{\partial z}+\frac{1}{\vartheta_\omega}\frac{\partial}{\partial t}\right)A_\omega &= \imath\frac{2\pi\omega^2\chi^2(\omega)\mu(\omega)}{c^2k_\omega}A_{2\omega}A_\omega^*\exp\left(-\imath\Delta k z\right)\\
\left(\widehat{k}_{2\omega}\frac{\partial}{\partial z}+\frac{1}{\vartheta_{2\omega}}\frac{\partial}{\partial t}\right)A_{2\omega} &= \imath\frac{2\pi(2\omega)^2\chi^2(2\omega)\mu(2\omega)}{c^2k_{2\omega}}A_\omega^2\exp\left(\imath\Delta k z\right)
\end{aligned} \tag{3}$$

where $\Delta k=2k_\omega-k_{2\omega}$, A_ω is the fundamental wave with frequency ω, and $A_{2\omega}$ is the second harmonic generated in the medium. Here, we consider the case where the refractive index is negative at the fundamental frequency ω and is positive at the second-harmonic frequency 2ω. The medium is considered to be loss-free, therefore, the refractive index for both frequencies is real-valued. Note that realistic metamaterials are lossy. Loss values are different for different frequency ranges. They are smaller in microwave range and quite high

in optical range. It should be mentioned that figure of merit for metamaterials is rapidly improving and recent paper [24] demonstrated feasibility of coherent compensation of losses by gain material embedded to nanostructures. In this paper we study fundamentals of second harmonic generation in negative index materials. We expect that differences from the case of conventional materials will be noticeable even in the idealized case of lossless material. The phase mismatch parameter Δk plays an important role for the spatial distribution of the electromagnetic field along the sample. In the next section we consider both $\Delta k = 0$ and $\Delta k \neq 0$. At the end of this paper we will briefly consider the effect of losses; detailed analysis will be presented in a separate publication.

III. CASE OF IDEAL PHASE MATCHING $\Delta k = 0$

We first consider second harmonic generation for continuous waves in a χ^2 medium under ideal phase matching conditions $\Delta k = 0$. The length of the sample we assume to be L. Using the symmetry properties of the susceptibility tensor χ^2 with respect to permutations of ω and 2ω frequencies, the mathematical model of second harmonic generation can be formulated in the following way [5, 6]:

$$\frac{dA_\omega}{dz} = -\imath \frac{2K\omega^2\mu(\omega)}{c^2 k_\omega} A_{2\omega} A_\omega^* \tag{4}$$

$$\frac{dA_{2\omega}}{dz} = \imath \frac{4K\omega^2\mu(2\omega)}{c^2 k_{2\omega}} A_\omega^2, \tag{5}$$

$$A_\omega(0) = A_\omega^0, \quad A_{2\omega}(L) = 0, \tag{6}$$

where $K = 2\pi\chi^2(2\omega)/c^2 = \pi\chi^2(\omega)/c^2$. Here we assume that there is no reflection at the ends of the sample. This effect is important at high pump wave intensities and for conventional materials they were studied in [25].

Let us represent the complex functions A_ω and $A_{2\omega}$ in terms of amplitudes $e_{1,2}$ and phases $\varphi_{1,2}$

$$A_\omega = e_1 \exp(\imath\varphi_1) \quad A_{2\omega} = e_2 \exp(\imath\varphi_2). \tag{7}$$

Substitution of Eqs. (7) into (4) and (5) , and separation of real and imaginary parts lead

to the following system of equations:

$$\begin{aligned}
\frac{de_1}{dz} &= \kappa e_1 e_2 \sin(\theta), \\
\frac{de_2}{dz} &= \kappa e_1^2 \sin(\theta), \\
\frac{d\theta}{dz} &= \kappa \left(\frac{e_1^2}{e_2} + 2e_2 \right) \cos(\theta),
\end{aligned} \tag{8}$$

with boundary conditions:

$$e_1(0) = e_{10}, \quad e_2(L) = 0. \tag{9}$$

Here θ and κ are defined as follows

$$\theta = \varphi_2 - 2\varphi_1, \quad \kappa = 4K\omega^2\mu(2\omega)/c^2 k_{2\omega}, \tag{10}$$

An n integral of motion [12] emerges from the first two equations:

$$e_1^2 - e_2^2 = m_1^2 = const \tag{11}$$

This integral of motion corresponds to the modified Manley-Row relation. Observe that while in case of second harmonic generation in conventional materials the Manley-Row relation is equivalent to conservation of energy ($e_1^2 + e_2^2 = const$), in our case, relation (11) corresponds to conservation of total flux of the energy. A second integral of motion for the system (8) reads as:

$$e_1^2 e_2 \cos(\theta) = m_2 = const. \tag{12}$$

The integral of motion (12) is consistent with boundary conditions (9) only if $\cos(\theta) = 0$. Taking into account that the pump wave energy should decay as it propagates forward in z, we conclude that the phase difference is equal to $\theta = 3\pi/2$, therefore the system of equations (8) can be represented as follows:

$$\frac{de_1}{dz} = -\kappa e_1 e_2, \quad \frac{de_2}{dz} = -\kappa e_1^2 \tag{13}$$

The solution of (13) has the following form

$$\begin{aligned}
e_1(\zeta) &= m_1 / \cos(m_1(l-\zeta)) \\
e_2(\zeta) &= m_1 \tan(m_1(l-\zeta))
\end{aligned} \tag{14}$$

here $\zeta = \kappa z$ and $l = \kappa L$. Solutions (14) contains unknown parameter m_1, which is the value of the fundamental field at the end of the sample. This parameter can be found from the boundary condition (9). Taking into account the Manley-Row relation (11), it all leads to the transcendental equation for m_1:

$$e_{10} = m_1 / \cos(m_1 l). \tag{15}$$

This equation can be solved numerically. The solution of (15) together with (14) determines the field distribution along the sample. The dependence of intensities e_1^2 and e_2^2 on ζ is represented in Fig.1 were the intensity boundary value $e_1^2(0)$ is chosen to be $e_{10}^2 = 3.5$, Here $l = 1$ and $m_1 = 1$.

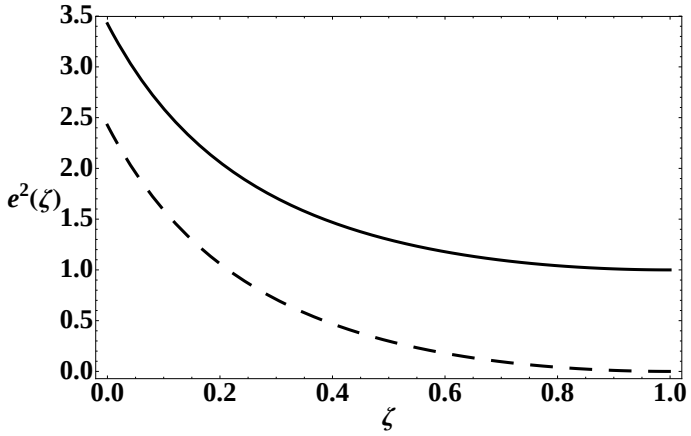

FIG. 1: The dependence of the intensity of fundamental wave e_1^2 (solid curve) and second harmonic e_2^2 (dashed curve) on the distance ζ with $e_{10}^2 = 3.5$

The solution of transcendental equation (15) for $l = 1$ is shown in Fig.2. This plot illustrates the dependence of the output field intensity $e_1(l) = m_1$, as a function of e_{10} (the amplitude of the fundamental field pumped into the medium). As shown in Fig.2, the formal solution of equation (15) has multiple branches. However, only the lower branch presented by a solid curve has physical meaning. Upper brunches represented by dashed curves are originated from periodicity of the cos function in (15). Both $e_1(\zeta)$ and $e_2(\zeta)$ corresponding to these branches have singularities on the interval $0 \leq \zeta \leq l$ which would be inconsistent with conservation of energy. Note that the lower "physical" branch shows saturation of output power of the electric field at the fundamental frequency $e_1(l)$ with increase of input power $e_1(0)$. This indicates that with the increase of input power $e_1(0)$ above 2, all excessive energy of the pump signal converts into energy of the second harmonic signal (see Fig. 3).

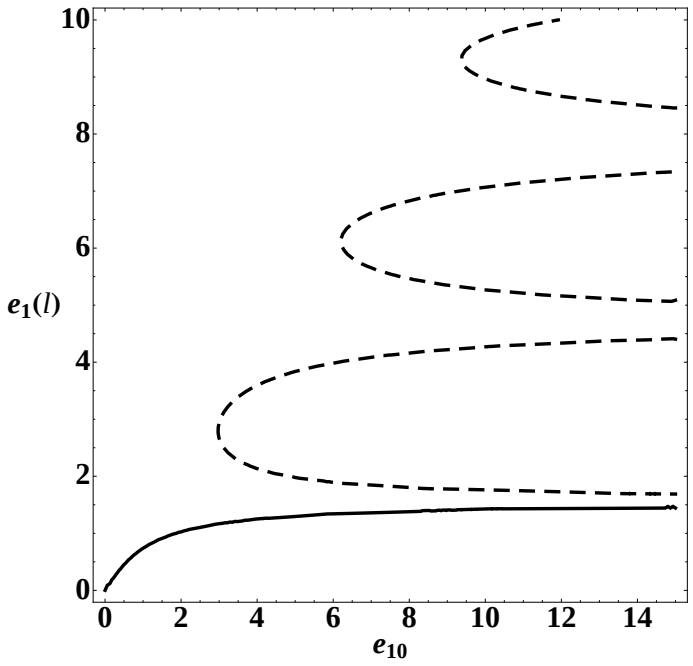

FIG. 2: The dependence of the intensity of output fundamental wave $e_1(l)$ on the e_{10}

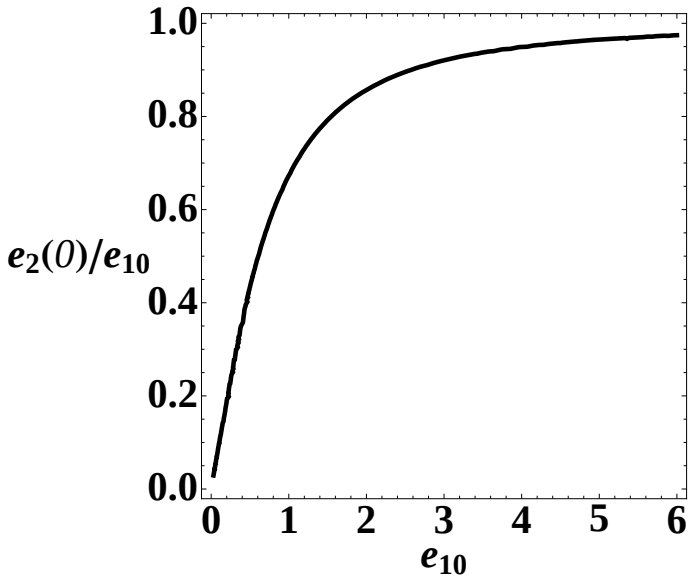

FIG. 3: The dependence of conversion efficiency of the pump to second harmonic fields.

The monotonic decay of the pump wave intensity along the sample, which is shown on Fig. (1), indicates that energy of the pump wave "flows" to the energy of second harmonic wave at every point along the sample. As we will show next, this unidirectional character of energy flow in the frequency domain is not uniform in the presence of phase mismatch.

IV. SECOND HARMONIC GENERATION IN THE PRESENCE OF A PHASE MISMATCH $\Delta k \neq 0$

Let us now consider the impact of phase mismatch Δk (Eq. (3)) on second harmonic generation. The system of equations describing the spatial distribution of field amplitudes $e_{1,2}(z)$ and phase difference $\theta(z)$ in the presence of phase mismatch reads:

$$\begin{aligned} \frac{de_1}{dz} &= \kappa e_1 e_2 \sin(\theta), \\ \frac{de_2}{dz} &= \kappa e_1^2 \sin(\theta), \\ \frac{d\theta}{dz} &= \kappa \left(\frac{e_1^2}{e_2} + 2e_2 \right) \cos(\theta) - \Delta k. \end{aligned} \tag{16}$$

Here $\theta = \varphi_2 - 2\varphi_1 - \Delta k z$ and κ is defined in (10). By introducing variables $\zeta = \kappa z$ and $l = \kappa L$ Eqs. (16) can be represented in the following form:

$$\begin{aligned} \frac{de_1}{d\zeta} &= e_1 e_2 \sin(\theta), \\ \frac{de_2}{d\zeta} &= e_1^2 \sin(\theta), \\ \frac{d\theta}{d\zeta} &= \left(\frac{e_1^2}{e_2} + 2e_2 \right) \cos(\theta) - \Delta, \end{aligned} \tag{17}$$

here $\Delta = \Delta k/\kappa$. The Manley-Row relation in this case remains unchanged:

$$e_1^2 - e_2^2 = m_1^2 = const, \quad m_1 = e_1(l).$$

and a second integral of motion in presence of phase mismatch reads:

$$e_2 e_1^2 \cos(\theta) + \frac{e_2^2 \Delta}{2} = m_2 = const \tag{18}$$

Taking into account the boundary condition $e_2(l) = 0$, we conclude that $m_2 = 0$ therefore

$$\cos(\theta) = -\frac{\Delta}{2} \frac{e_2}{(m_1^2 + e_2^2)} \tag{19}$$

The function (19) has an extremum at $e_2^2 = m_1^2$ and $\cos(\theta)$ at this value of e_2 gives $\cos(\theta) = -\Delta/4m_1$. Given that $|\cos(\theta)| \leq 1$, there is the critical value of mismatch $|\Delta_{cr}| = 4m_1$ such that $\max|\cos\theta| = 1$. Notice that (19) is defined for arbitrary values of e_2 if $|\Delta| \leq 4m_1$. If $|\Delta| \geq 4m_1$ then there is a forbidden gap for values of e_2:

$$\frac{1}{4}\left(|\Delta| - \sqrt{\Delta^2 - \Delta_{cr}^2} \right) < e_2 < \frac{1}{4}\left(|\Delta| + \sqrt{\Delta^2 - \Delta_{cr}^2} \right). \tag{20}$$

In this case $|\cos\theta| \leq 1$ if

$$e_2 \geq \frac{1}{4}\left(|\Delta| + \sqrt{\Delta^2 - \Delta_{cr}^2}\right) \tag{21}$$

$$0 \leq e_2 \leq \frac{1}{4}\left(|\Delta| - \sqrt{\Delta^2 - \Delta_{cr}^2}\right). \tag{22}$$

Since the value of e_2 on the right side of the sample is set to be zero ($e_2(l) = 0$), the branch of e_2 values (21) is not accessible. Values of e_2 in this case remain within the range (22). In this case the conversion efficiency of the pump wave to second harmonic is limited by the value $4e_{10}/(|\Delta| - \sqrt{\Delta^2 - 16m_1^2})$. The dependence of $f(\theta) = -\Delta e_2/2(m_1^2 + e_2^2)$ on e_2 for different values of mismatch is shown in Fig. 4. The bold curve on this figure corresponds to the critical value of the mismatch. The forbidden gap for e_2 can be seen for two lowest curves, when curves are below -1. The presence of a forbidden gap for

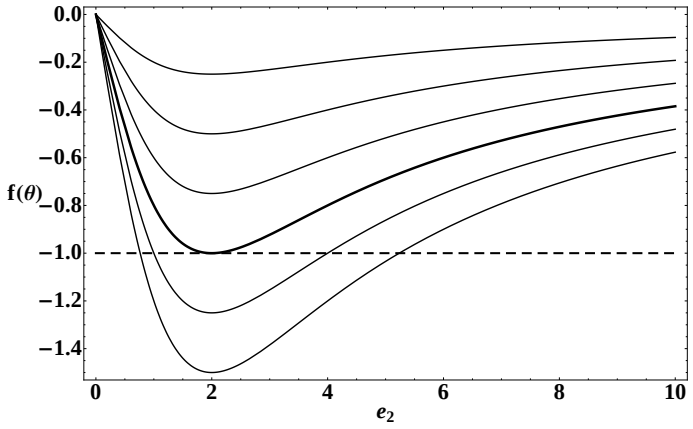

FIG. 4: The dependence of the $f(\theta)$ on e_2 with different values of $\Delta = k \times m_1$, here $k = 1, 2, \ldots, 6$ and $m_1 = 1.2$. The bold curve corresponds to a critical value of $\Delta = \Delta_{cr}$

e_2 suggests the existence of two types of solutions for e_2. The first type corresponds to mismatch values $|\Delta| \leq 4m_1$ and in this case e_2 is not bounded from above. This means that the conversion rate of fundamental to second harmonic, can in principle, be high (close to 1 - ideal conversion, similar to Fig. 3 in the previous section). The second type of solutions correspond to mismatch values $|\Delta| \geq 4m_1$; in this case the amplitude e_2 is bounded from above $0 \leq 4e_2 \leq |\Delta| - \sqrt{\Delta^2 - 16m_1^2}$. This means that there is a limitation of the output intensity of second harmonic field with respect to the growing input intensity of fundamental harmonic.

For further considerations, it is more convenient to deal with field intensities rather then with amplitudes. Using expression (19) for $\cos(\theta)$, the second equation of (17) can be

represented as an equation for the intensity $P_2 = e_2^2$:

$$\frac{dP_2}{d\zeta} = \{F(P_2)\}^{1/2}, \tag{23}$$

where $F(P_2)$ is a cubic polynomial

$$F(P_2) = 4P_2^3 + \left(8m_1^2 - \Delta^2\right) P_2^2 + 4m_1^4 P_2.$$

with the following roots:

$$\begin{aligned} P_{2c} &= \frac{1}{8}\left(\Delta^2 - 8m_1^2 + \Delta\sqrt{\Delta^2 - 16m_1^2}\right) \\ P_{2b} &= \frac{1}{8}\left(\Delta^2 - 8m_1^2 - \Delta\sqrt{\Delta^2 - 16m_1^2}\right) \\ P_{2a} &= 0. \end{aligned} \tag{24}$$

Notice that these roots (24) define the forbidden gap $[\sqrt{P_{2b}}, \sqrt{P_{2c}}]$ for values of e_2 (see Fig. 4 and equations (21), (22)).

Based on this qualitative analysis, we conclude that there are three regimes of second harmonic generation controlled by the absolute value of the phase mismatch. In the following subsection we will analyse solutions describing spatial field distribution inside the sample.

A. Three regimes of second harmonic generation

The absolute value of the phase mismatch defines three different regimes of second harmonic generation: $|\Delta| < \Delta_{cr}$, $|\Delta| = \Delta_{cr}$ and $|\Delta| > \Delta_{cr}$. First we consider the case of subcritical mismatch: $|\Delta| < \Delta_{cr}$.

1. Subcritical mismatch

In the case where $|\Delta| < \Delta_{cr}$, roots (24) are complex-valued and the solution of (25) can be expressed in terms of Weierstrass functions $\wp$ [27]. By expanding $F(P_2)$ in Taylor series and introducing a new variable:

$$s = \frac{F'(P_{2a})}{4(P_2 - P_{2a})} + \frac{1}{24}F''(P_{2a}).$$

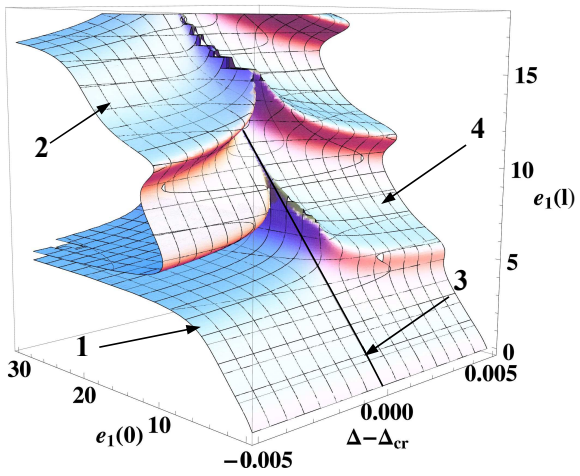

FIG. 5: The dependence of the output field amplitude $e_1(l)$ at the fundamental frequency on e_{10} near the critical value of phase mismatch Δ_{cr}

where derivatives of the polynomial are taken with respect to P_2. With htis transformation, the solution of equation (23) can be represented in implicit form:

$$\zeta - l = \int_s^\infty \frac{ds}{\left\{4s^3 - g_2 s - g_3\right\}^{1/2}}, \tag{25}$$

where g_2 and g_3 are invariants of the Weierstrass function.

$$g_2 = \frac{1}{12}\left(8m_1^2 - \Delta^2\right)^2 - 4m_1^4, \quad g_3 = \frac{1}{3}m_1^4\left(8m_1^2 - \Delta^2\right) - \frac{1}{216}\left(8m_1^2 - \Delta^2\right)^3.$$

Finally, the amplitudes of fundamental and second harmonics have the following form:

$$e_1(\zeta) = \sqrt{m_1^2 + e_2^2(\zeta)}, \tag{26}$$

$$e_2(\zeta) = \frac{m_1^2}{\sqrt{\left(\wp(l-\zeta; g_2, g_3) - \left(8m_1^2 - \Delta^2\right)/12\right)}} \tag{27}$$

The parameters g_2 and g_3 are functions of Δ and m_1. To determine solutions of Eqs. (17) we need to solve for the unknown value of the output pump wave m_1. The value of m_1 can be found taking into account the output boundary condition $m_1 = e_1(l)$ and the Manley-Row relation (11), which lead to the following transcendental equation for m_1:

$$e_{10}^2 = m_1^2 + \frac{m_1^4}{\wp(l; g_2, g_3) - \left(8m_1^2 - \Delta^2\right)/12} \tag{28}$$

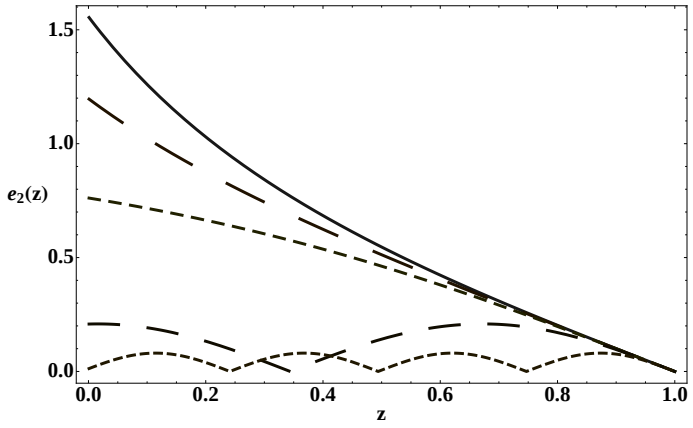

FIG. 6: The dependence of second harmonic's amplitude $e_2(\zeta)$ on the ζ with different values of phase mismatch(the solid curve: $\Delta = 0$, large dashed curve $\Delta = 2m_1$, small dashed curve: $\Delta_{cr} = 4m_1$, intermediate dashed curve: $\Delta = 10m_1$, doted curve: $\Delta = 25m_1$).

To determine the unknown parameter $m_1 = e_1(l)$, Eq.(28) needs to be solved numerically. The analysis of the $e_1(l)$ dependence on e_{10} and Δ shows that with increasing phase mismatch from 0 to Δ_{cr}, all branches (physical and nonphysical) shift upwards and nonphysical branches change their shapes. Fig. 5 shows the dependence of the output field amplitude $e_1(l)$ at fundamental frequency on e_{10} near the critical value of phase mismatch Δ_{cr}. The sheet, labeled as "1", corresponds to the physical branch, while the sheet labeled as "2" represents the first nonphysical branch. Other nonphysical sheets are located above the nonphysical sheet "2" as shown on Fig. 5. The spatial distribution of $e_1(\zeta)$ and $e_2(\zeta)$ can be obtained by substitution of the solution of the Eq. (28) (m_1) in Eqs. (26) and (27). We found that all solutions $e_1(\zeta)$ and $e_2(\zeta)$ are monotonically decreasing in ζ. An example of $e_2(\zeta)$ at $\Delta = \Delta_{cr}/2$ is shown in Fig. 6).

The conversion efficiency $\alpha = e_2(l)/e_{10}$ as a function of the input amplitude e_{10} is presented in Fig. 11. As one can observe, α is approaching its asymptotic optimal value $\alpha = 1$ in slower fashion for larger values of $|\Delta|$.

2. Critical mismatch

When the value of phase mismatch is critical $|\Delta| = \Delta_{cr}$, the roots $P_{2c} = P_{2b} = \Delta_{crit}^2/16 = m_1^2$ and the discriminant of the Weierstrass function is zero. In this case, the function $\wp(l - \zeta; g_2, g_3)$ can be represented in terms of hyperbolic functions. Thus the Eqs. (26)

and (27) take the form:

$$e_1(\zeta) = \sqrt{m_1^2 + e_2^2(\zeta)} \tag{29}$$

$$e_2(\zeta) = m_1 \tanh\left(m_1(l-\zeta)\right) \tag{30}$$

and the transcendental equation for m_1 reads as

$$e_{10}^2 = m_1^2\left(1 + \tanh^2\left(m_1 l\right)\right) \tag{31}$$

The numerical solution of Eq. (31) is shown in Fig.5 (line "3"). Observe that at large values of e_{10}, the solution of Eq. (31) is proportional to e_{10} ($m_1 \approx e_{10}$). Therefore, at large values of e_{10} the conversion efficiency $\alpha \to \tanh(le_{10})$ is always less then one while in the subcritical regime $\alpha \to 1$ (see Fig. 11).

At this point we can conclude that in both the subcritical and critical regimes, energy uniformly flows from fundamental to second harmonic, which is similar to the case of ideal phase matching. Therefore, in contrast to the classical case of second harmonic generation, efficient energy conversion in negative index materials takes place not only for ideal phase matching, but for the entire interval of phase mismatch values: $|\Delta| \leq \Delta_{cr}$. This gives more flexibility from the point of view arranging phase matching condition to observe efficient second harmonic generation in negative index materials.

3. Overcritical mismatch

At large mismatch values, when $|\Delta| > \Delta_{cr}$, all roots of (24) are real. In this case it is convenient to represent $\wp(l-\zeta; g_2, g_3)$ in terms of Jacobi elliptic sn function [26]. Eqs (26) and (27) can be represented as

$$e_1(\zeta) = \sqrt{m_1^2 + e_2^2(\zeta)} \tag{32}$$

$$e_2(\zeta) = \sqrt{P_{2b}}\ \mathrm{sn}\left[\sqrt{P_{2c}}(l-\zeta), \gamma\right], \tag{33}$$

here $\gamma = \sqrt{P_{2b}/P_{2c}}$, and the equation for m_1 takes the following form:

$$e_{10}^2 = m_1^2 + P_{2b}\ \mathrm{sn}^2\left[\sqrt{P_{2c}}l, \gamma\right] \tag{34}$$

The sheet corresponding to solutions of (34) is labeled in Fig. 5 as "4". In contrast to the subcritical regime, all solutions in this case are represented by a single sheet. This sheet has

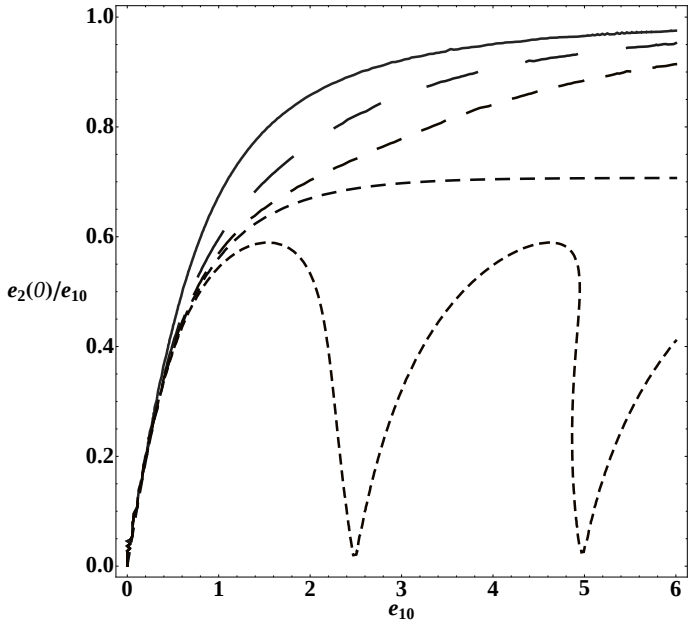

FIG. 7: Dependence of conversion efficiency $\alpha = e_2(0)/e_{10}$ on input field amplitude e_{10} with different values of phase mismatch Δ: Solid curve $\Delta = 0$; large dashed curve $\Delta = 3.5m_1$; dashed curve $\Delta = 3.9m_1$; small dashed curve $\Delta_{cr} = 4m_1$; doted oscillation curve $\Delta = 4.5m_1 > \Delta_{cr}$

folds, hence the intersection of this sheet with the plane corresponding to $\Delta = const$ gives multivalued dependance of $e_1(l)$ on e_{10}. This dependance for two different values of Δ is shown in Fig. 8.

In the supercritical regime the second harmonic field experiences spatial periodic oscillations with period $4\mathbf{K}(\gamma)$ (see Fig. 6). These spatial periodic oscillations is an indication of dual energy exchange between fundamental and second harmonics. Direction of energy flow is periodically changing along the sample.

The distance between neighboring zeros $\tilde{\zeta}$ of the amplitude of second harmonic is determined by the following formula:

$$\tilde{\zeta} = \frac{2\mathbf{K}(\gamma)}{\sqrt{P_{2c}}} \tag{35}$$

If the slab length satisfies the condition $l = n \times \tilde{\zeta}$ $(n = 1, 2, 3 \ldots)$, then the amplitude of the second harmonic wave is zero at the both ends of the slab (zero conversion efficiency). Therefore such slab is transparent for the pump wave frequency. A plot of the transmission coefficient $\Im = e_1(l)^2/e_{10}^2$ as function of e_{10} is shown in Fig.9. The transmission coefficient is equal to 1 at the points labeled as "1", "2", ... (transmission resonances). The spatial

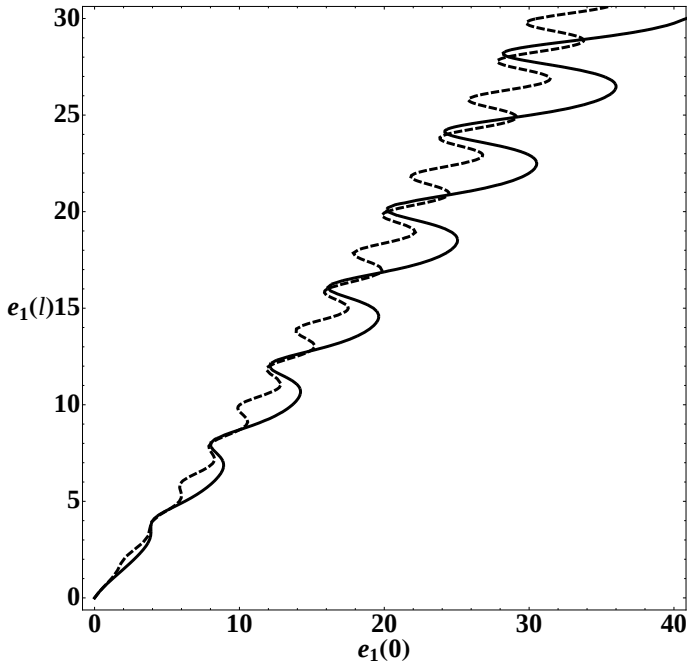

FIG. 8: The dependence of the output field amplitude $e_1(l)$ at fundamental frequency on e_{10}. Solid curve $\Delta = 4.1m_1$, dashed curve $\Delta = 4.5m_1$

distribution of the fundamental and second harmonic fields corresponding to the transmission resonance at the point "1" (see Fig.9) is shown in Fig.10.

In practice negative index metamaterials are lossy. The presence of losses can affect the value of critical mismatch, however it does not change the unidirectional character of energy flow in negative index materials that takes place in critical and subcritical regimes. That is, for the entire interval of mismatch values $|\Delta| \leq \Delta_{cr}$. Therefore, the presence of losses does not eliminate the fundamental difference of second harmonic generation in negative index versus conventional materials. In other words losses change equation (17) simply by adding of $-\beta_1 e_1$ and $\beta_2 e_2$, to the first two equations and leaving the third equation for the phase θ along. Since $e_{1,2}$ are two amplitudes of electric fields the factor multiplying $\cos\theta$ in that equation can never become negative regardless of wether amplitude dynamics is conservative or damped. In particular, zero crossings on the right hand side of this equation still take place for sufficiently large mismatch values. Note that the subcritical regime corresponds to absence of zero crossings and supercritical regime corresponds to the presence of zero crossings.

An example of spatial profiles for e_1 and e_2 corresponding to the subcritical regime at

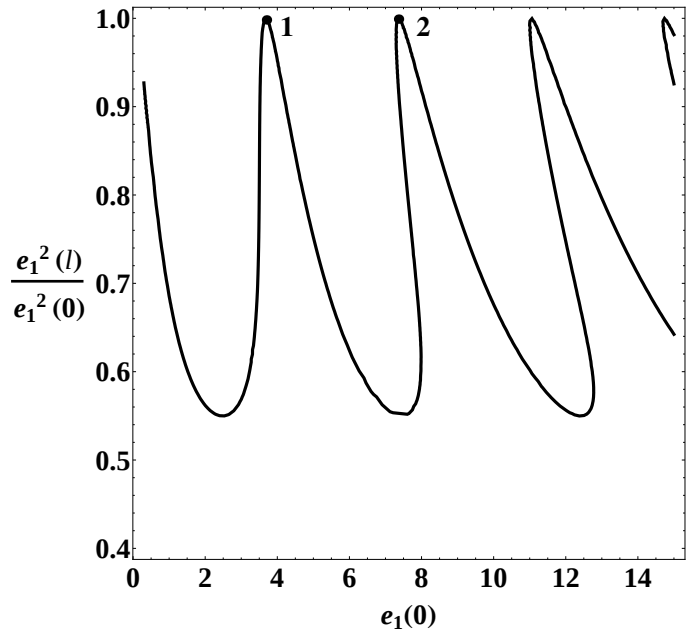

FIG. 9: Dependence of the transmission coefficient $\Im$ on pumped field amplitude e_{10}. $\Delta = 4.2m_1$

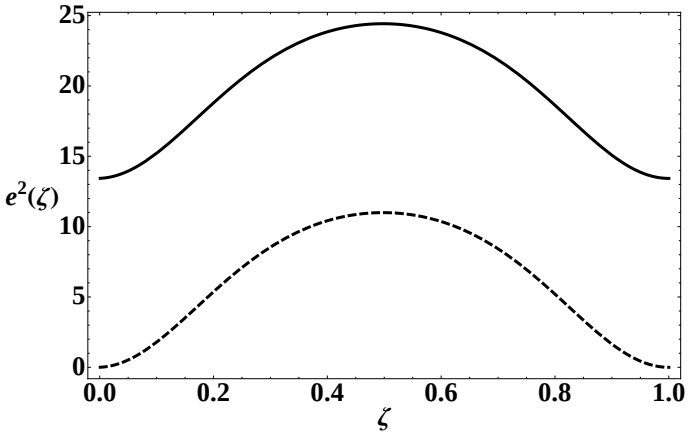

FIG. 10: Spatial distribution of the intensities $e_1^2(\zeta)$ (solid curve) and $e_2^2(\zeta)$ (dashed curve) inside the slab

$e_{10}^2 = 1$ is shown in Fig. (12). Linear losses for fundamental and second harmonic fields β_1 and β_2 are chosen to be: (i) solid curves - $\beta_1 = 0.03$, $\beta_2 = 0.01$; (ii) dashed curves - $\beta_1 = 0.06$, $\beta_2 = 0.01$; (iii) dashed-doted curves - $\beta_1 = 0.1$, $\beta_2 = 0.01$. Fig. (12) illustrates energy transfer along the sample from fundamental to second harmonic in the presence of nonzero mismatch. Losses lead to faster decay of amplitude of fundamental harmonic and lower values of second harmonics amplitude at larger loss values. Spatial profiles for e_1 and e_2 corresponding to overcritical regime with losses at $e_{10}^2 = 1$ and $\Delta = 3$ is shown in Fig. (13).

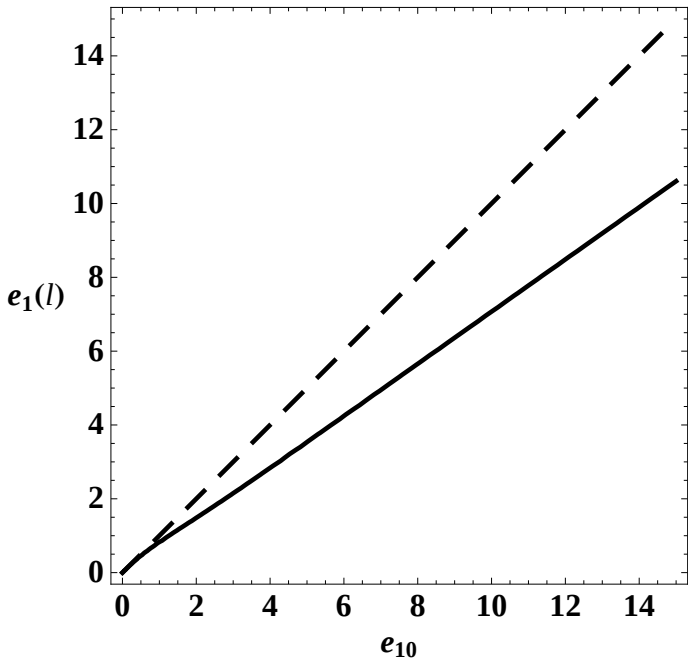

FIG. 11: Dependence of conversion efficiency $\alpha = e_2(0)/e_{10}$ on input field amplitude e_{10} with different values of phase mismatch Δ: Solid curve $\Delta = 0$; large dashed curve $\Delta = 3.5m_1$; dashed curve $\Delta = 3.9m_1$; small dashed curve $\Delta_{cr} = 4m_1$; doted oscillation curve $\Delta = 4.5m_1 > \Delta_{cr}$

Solid curves in Fig. (13) correspond to $\beta_1 = 0.03$ and $\beta_2 = 0.01$, dashed curves correspond to $\beta_1 = 0.06$ and $\beta_2 = 0.01$, finally dashed-doted curves correspond to $\beta_1 = 0.1$, $\beta_2 = 0.01$. The presence of losses in the overcritical regime does preserve the oscillatory behavior of the fields but not longer in a periodic fashion along the sample. The insert shows a zoomed-in fragment of the e_2 spatial profile. Fig. (13) clearly illustrates the effect of fields energy loss due to absorption. Further detailed analysis of the impact of losses on second harmonic generation in negative index materials will be presented in a separate publication.

V. CONCLUSION

We considered second harmonic generation in negative index materials. Specifics of this process is in the negative value of the refractive index for the pump wave and the positive value for the second harmonic. This led to important features which are different from the case of second harmonic generation in conventional dielectrics. The main difference is in the existence of nonzero critical values of the phase mismatch. If the absolute value of phase

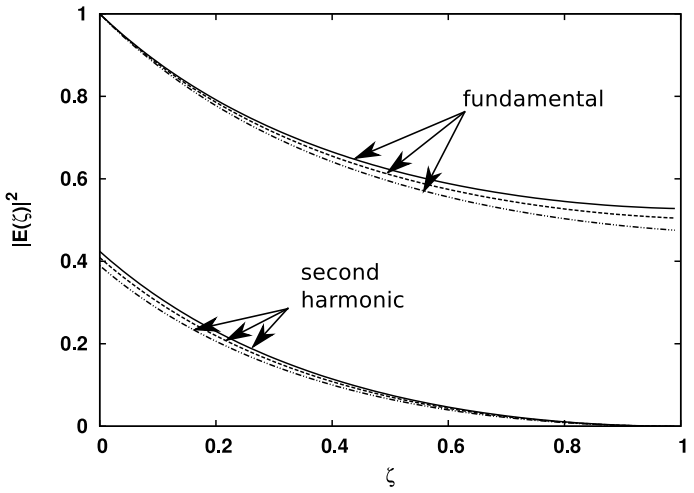

FIG. 12: The dependence of the intensity of fundamental wave e_1^2 and second harmonic e_2^2 on the distance ζ with $e_{10}^2 = 1$, $\Delta = 0.75$ for three sets of absorption coefficient values $\beta_1 = 0.03,\ 0.06,\ 0.1$ and $\beta_2 = 0.01$ for all three cases. Corresponding lines are solid, dashed and dot-dashed lines respectively.

mismatch is below critical, then the fundamental field intensity is monotonically decaying along the sample leading to efficient frequency conversion. When the absolute value of phase mismatch exceeds a critical value, theis monotonic decay of intensities transforms to a spatial periodic oscillations. Note, that in the conventional case the critical value of phase mismatch is zero.

Another important feature is the dependance of conversion efficiency on the amplitude of the incident pump wave. When the absolute value of phase mismatch is below critical value, then the conversion efficiency asymptotically approaches 100% at large values of the incident pump wave amplitude. It should be stressed that in this case the asymptotic value of conversion efficiency does not depend on the phase mismatch value. The phase mismatch affects only the rate of approaching of conversion efficiency to its asymptotic value. When the phase mismatch is exactly equal to critical value, then the asymptotic value of conversion efficiency experiences a jump to a value which is less than 100%. When the absolute value of phase mismatch is above critical value, the conversion efficiency becomes an oscillatory function of the incident pump wave amplitude.

Finally, we found that the dependance of output amplitude of the pump wave on its input amplitude is single valued if the absolute value of phase mismatch is below critical

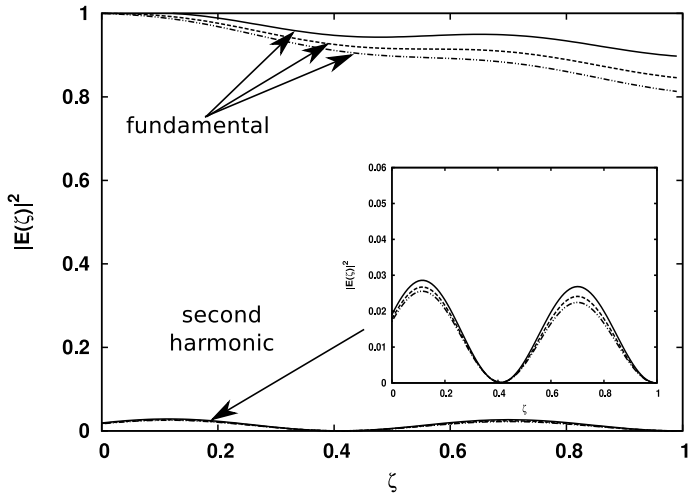

FIG. 13: The dependence of the intensity of fundamental wave e_1^2 and second harmonic e_2^2 on the distance ζ with $e_{10}^2 = 1$, $\Delta = 3$ for three set of values for absorption coefficients $\beta_1 = 0.03$ and $\beta_2 = 0.01$; $\beta_1 = 0.06$ and $\beta_2 = 0.01$; and $\beta_1 = 0.1$, $\beta_2 = 0.01$. These cases are presented by solid, dashed and dot-dashed lines respectively. Insert shows zoomed-in fragment of e_2 spatial profile.

and becomes multi-valued in the opposite case.

Acknowledgments

We would like to thank V.P. Drachev, A. K. Popov and V. M. Shalaev for valuable discussions and A. Aceves for help during preparation of this paper. A.I.M and Zh.K. appreciate support and hospitality of the University of Arizona Department of Mathematics during the preparation on this manuscript. This work was partially supported by NSF (grant DMS-0509589), ARO-MURI award 50342-PH-MUR and State of Arizona (Proposition 301), RFBR (grant No. 09-02-00701-a) and the Federal Goal-Oriented Program "Scientific and Scientific-Educational Personnel of Innovational Russia".

---

[1] R. Shelby, D. R. Smith and S. Schultz, Science, 292, (2001) 77.

[2] V. M. Shalaev, W. Cai, U. K. Chettiar, H. Yuan, A. K. Sarychev, V. P. Drachev, A. V. Kildishev, Opt. Lett. 30, 3356 (2005).

[3] S. Zhang, W. Fan, C. Panoiu, K. J. Malloy, R. M. Osgood, S. R. Brueck, Phys. Rev. Lett. 95, 137404 (2005).

[4] A. K. Sarychev and V. M. Shalaev, Electrodynamics of Metamaterials, World Scientific, Singapore, 2007

[5] Y.R. Shen The principles of non-linear optics (John Wiley Sons, New York, Chicester, Brisbane, Toronto, Singapore, 1984).

[6] R.W. Boyd, Nonlinear optics,(Academic Press, Boston 1992).

[7] V.M. Agranovich, Y.R. Shen, R.H. Baughman, and A.A. Zakhidov, Phys. Rev. B: Condens. Matter Mater. Phys., **69**, 165 112, (2004)

[8] N. Mattiucci, G. DAguanno, M. Scalora, M.J. Bloemer, Physical Review E, **72**, 066612 (2005)

[9] G. DAguanno, N. Mattiucci, M. Scalora, and M.J. Bloemer, Physical Review E, **73**, 036603 (2006)

[10] G. DAguanno, N. Mattiucci, M. Scalora, and M.J. Bloemer, Physical Review E **74**, 026608 (2006)

[11] N.M. Litchinitser, I.R. Gabitov, A.I. Maimistov, V.M. Shalaev, Negative refractive index metamaterials in optics, Progress in Optics, Volume **51**, Chapt.1, p. 1-67 (2008). Edited by E. Wolf , Elsevier, 481 pp. ISBN: 978-0-444-53211-4.

[12] A. K. Popov, V. M. Shalaev, Negative-Index Metamaterials: Second-Harmonic Generation, Manley-Rowe Relations and Parametric Amplification, Appl. Phys. B. 2006,

[13] J.A. Armstrong, N. Bloembergen, J. Ducuing and P.S. Pershan , Interactions between light waves in a nonlinear dielectric, Phys. Rev. 127, 1918 1939, 1962.

[14] V.M. Agranovich and Yu.N. Gartshtein, Usp. Fiz. Nauk, **176**, p. 1051, (2006)

[15] V.P. Drachev, W. Cai, U. Chettiar et al., Laser Phys. Lett., **3**, p. 49, (2006)

[16] W. Cai, U.K. Chettiar, H.-K. Yuan et al., Opt. Express, **15**, p. 3333, (2007)

[17] I.V. Shadrivov, A.A. Zharov and Yu.S. Kivshar, J. Opt. Soc. Am. B: Opt. Phys., **23**, p. 529, (2006)

[18] A.K. Popov, V.V. Slabko and V.M. Shalaev, Laser Phys. Lett., **3**, p. 293, (2006)

[19] A.K. Popov and V.M. Shalaev, Appl. Phys. B, **84**, p. 131, (2006).

[20] A. K. Popov and Vladimir M. Shalaev, Opt. Lett. **31**, 2169-2171 (2006)

[21] A.K. Popov and V.M. Shalaev, Journal Applied Physics B: Lasers and Optics Publisher **84**, 131-137 (2006)

[22] A.I. Maimistov, I.R. Gabitov and E.V. Kazantseva, Opt. Spektrosk., **102**, p. 99 (2007) [Opt. Spectrosc. (Engl. Transl.), **102**, p. 90].

[23] V. Roppo, C. Ciraci, C. Cojocaru, and M. Scalora, JOSAB, **27**, p. 1671–1679, (2010)

[24] S.Xiao, V.P. Drachev, A.V. Kildishev, X. Ni, U. K. Chettiar, H.-K. Yuan, and V.M. Shalaev, Nature **466**, p. 735-738 (2010)

[25] V.P. Drachev, S.V. Perminov, V.P. Safonov, Optics Communications, **130**, p. 402-412, (1996)

[26] Lavrentev M.A., Shabat B.V. Complex analysis, Moscow, 1951 (in russian).

[27] Whittaker ET, Watson G. A course of modern analysis. Cambridge: Cambridge University Press; 1988.